Available online at www.sciencedirect.com
ScienceDirect
Mendeleev Commun., 2016, **26**, 32–34
Mendeleev Communications

Plasmonic properties of aged silver hydrosols

Anna A. Semenova,[a] Nadezhda A. Braze,[b] Georgy V. Maksimov,[b] Irina A. Semenova,[c] Alexander P. Semenov[c] and Eugene A. Goodilin*[a,d,e]

[a] *Department of Materials Science, M. V. Lomonosov Moscow State University, 119991 Moscow, Russian Federation. Fax: +7 495 939 0998; e-mail: goodilin@yandex.ru, goodilin@inorg.chem.msu.ru*
[b] *Department of Biology, M. V. Lomonosov Moscow State University, 119991 Moscow, Russian Federation*
[c] *Institute of Physical Materials Science, Siberian Branch of the Russian Academy of Sciences, 670047 Ulan-Ude, Russian Federation*
[d] *Department of Chemistry, M. V. Lomonosov Moscow State University, 119991 Moscow, Russian Federation*
[e] *N. S. Kurnakov Institute of General and Inorganic Chemistry, Russian Academy of Sciences, 119991 Moscow, Russian Federation*

DOI: 10.1016/j.mencom.2016.01.013

The strongest plasmonic band in UV-VIS absorption spectra is commonly supposed to be a sole characteristic of the optical properties of silver hydrosols determining their effectiveness in surface enhanced Raman spectroscopy (SERS). However, we found that the real enhancement coefficients of SERS correlate well with the contribution of the smallest nanoparticles rather than with overall light absorption as a feature of the whole ensemble of the nanoparticles of all fractions.

The surface enhanced Raman spectroscopy (SERS) materials are of great current interest[1–13] as principally new analytical tools for environmental chemistry and biomedical diagnostics.[14–19] Almost all known preparation techniques of silver nanoparticles yield plasmonic nanoparticle ensembles with different size distribution functions; however, they are traditionally characterized by the medium size of nanoparticles. In these terms, UV-VIS spectroscopy is often used as a simple test for the presence of nanoparticles.[17–19] However, this optical characterization seems to reflect nanoparticle properties in a complicated manner in the case of polydispersed ensembles of nanoparticles.[17–19] Indeed, the energetic positions of plasmon resonance bands in the optical spectrum is substantially affected by the material, size, shape, and dielectric surrounding of nanoparticles; thus, the optical spectra contain important but not self-sufficient structural information.[15,19]

In this work, we prepared a number of typical silver nanoparticle sols in accordance with the Leopold and Lendl[14] procedure by varying the temperature in a range of 25–60 °C with post-preparation ageing for two months; then, the samples were investigated in detail to discover key features for the SERS studies of biology-related objects.

The Leopold and Lendl procedure is based on the reduction of silver nitrate in alkaline aqueous solutions by hydroxylamine hydrochloride, and such sols are a typical example of materials for SERS measurements. The size distribution functions of the sols are bimodal (Figures 1, 2); moreover, the distribution function parameters shift in time in a complicated manner even on storage at 4 °C thus leading to different absorption spectra (Figure 2). The preparation route yields a silver phase in a form of either rounded nanoparticles with a small admixture of anisotropic rods or platelets (Figure 1). A typical size of the isotropic nanoparticles was 10–100 nm depending on the preparation temperature and ageing time of the hydrosols (Figures 1, 2). The nanoparticles are mostly polyhedral and demonstrate pentagonal capping typically appeared for this system due to twinning.[2,3,7,8] The particle size distribution is not uniform, as evident from the TEM data, and DLS estimates silver particle sizes below 200 nm [Figure 1(*b*)]. In particular, room temperature preparation affords 10 nm spherical nanoparticles, while other samples contain larger elongated particles.

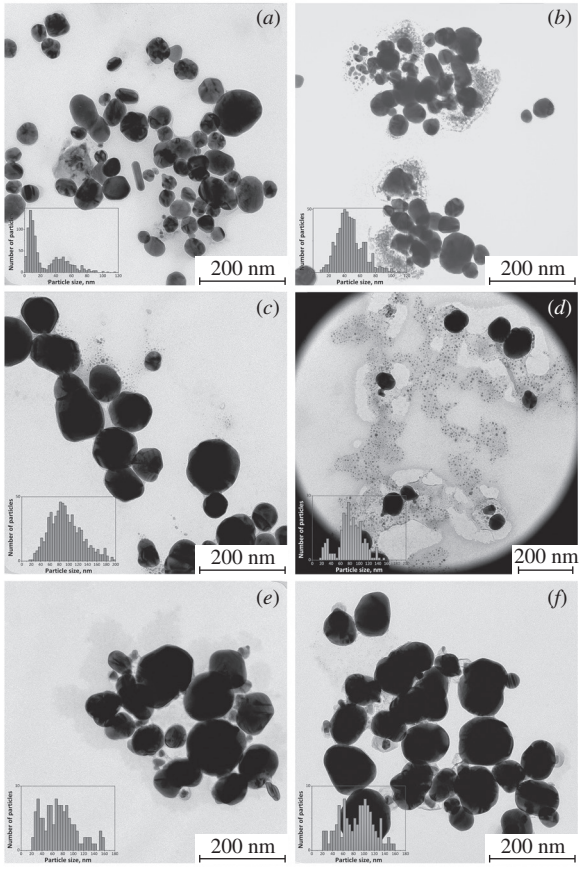

Figure 1 Microstructures of as-prepared and aged silver nanoparticle ensembles [transmission electron microscopy (TEM), LEO912 AB OMEGA (Carl Zeiss)]. (*a*), (*c*), (*e*) The samples prepared at 25, 40 and 60 °C, respectively. (*b*), (*d*), (*f*) The same samples after ageing for two months. The insets show particle distribution functions for 200+ particles counted.

An increase in either the preparation temperature or the ageing time produces the red shift of the plasmonic band position by about 50 nm and decreases the absorption intensity of the nanoparticle ensemble [Figure 2(*a*)]. The DLS [Figure 2(*b*)] and TEM

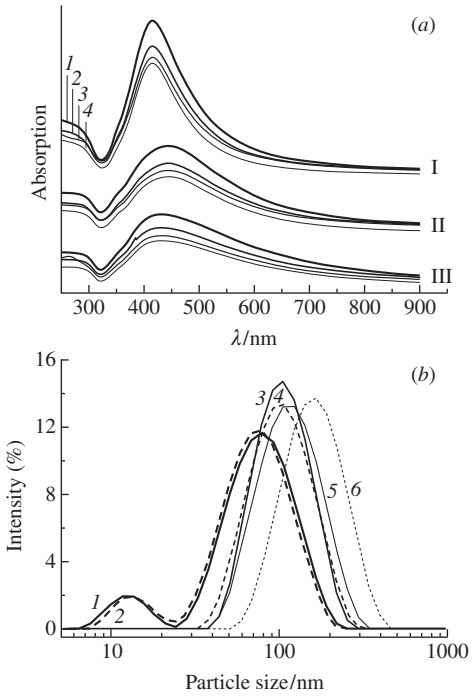

Figure 2 Characteristics of particle distribution functions of hydrosols and their optical properties. (*a*) UV-VIS absorption spectra; I, II and III – samples prepared at 25, 40 and 60 °C, respectively [Lambda 35 (Perkin-Elmer)]; ageing times, (*1*) a day, (*2*) a week, (*3*) a month and (*4*) two months. (*b*) Particle size distribution (Malvern Zetasizer Nano ZS instrument; 25 °C; He–Ne laser, 4 mW; wavelength, 632.8 nm; beam diameter, 0.63 nm). The scattering and detection angles were 175 and 12.8°, respectively. The samples were placed in standard Malvern zeta potential disposable capillary cells and polystyrene cuvettes for zeta potential and size measurements, respectively. All the measurements were repeated several times. (*1*) The sample prepared at room temperature, (*2*) the same sample, aged for two months, (*3*), (*4*) preparation at 60 °C and ageing for two months, (*5*), (*6*) a similar group prepared at 60 °C.

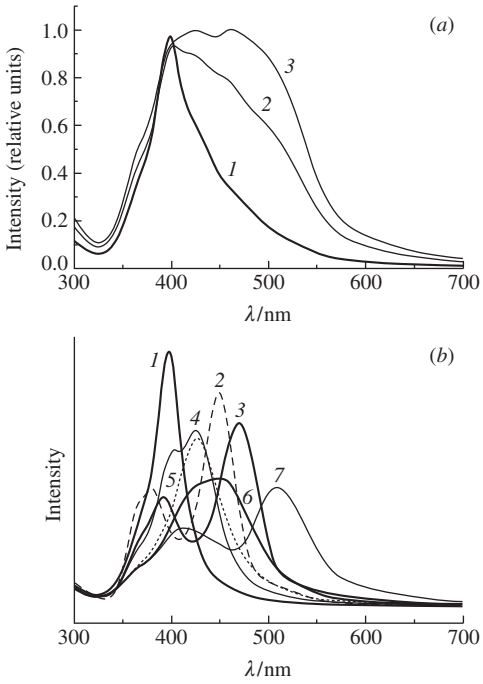

Figure 3 Discrete dipole approximation of the simulated extinction spectra of nanoparticle ensembles with different contributions of rounded and slightly elongated silver particles. (*a*) Plasmonic bands for a mixture of 70×70×105, 40×40×60, 70×70×84, 40×40×48 nm ellipsoids and 10 nm spheres with contributions (%) of (*1*) 10:10:10:30:50, (*2*) 35:10:35:10:10 and (*3*) 50:20:20:10:0. (*b*) Spectral components of the simulated spectra: (*1*) 10 and (*5*) 70 nm spheres, (*2*) 10×10×15 nm, (*3*) 40×40×60 nm, (*4*) 40×40×48 nm, (*6*) 70×70×84 and (*7*) 70×70×105 nm ellipsoids (DDA method based on the DDSCAT 7.1 software[15] for aqueous surrounding and the number of dipoles of 6×10^4–9×10^4).

data (Figure 1, insets) evidence for a gradual increase in the medium size and a decrease in the contribution of 10 nm particles probably due to the Ostwald ripening. Thus, the experimentally obtained nanoparticle ensembles exhibit a wide distribution of particle sizes and shapes leading to an inhomogeneous broadening of the resulting plasmon resonance peaks.

Each nanoparticle makes its own contribution to the extinction spectrum in dilute sols independently of the neighboring particles. This assumption gives a possibility to compute the extinction spectrum of the particle ensemble additively as the sum of individual particle contributions. The discrete dipole approximation method[15,16] is a useful and versatile computational tool for testing the absorption, scattering and extinction properties of nanoparticles with arbitrary shapes. Some experimental results of such a simulation are displayed in Figure 3.

First, it is obvious that any ensemble of spherical particles does not physically give a broad extinction spectrum observed experimentally (Figure 2) since isotropic particles possess a very narrow plasmon peak; moreover, this narrow peak is red shifted by only 15–20 nm even if the particle size becomes several times larger.[17–19] Figure 3(*a*) shows that the peak of 10 nm spherical particles is located at about 400 nm, as is well known. Much larger, almost isotropic 40×40×48 ellipsoids have two peaks at about 405 and 425 nm; therefore, even a small anisotropy gives already a contribution to the red-shifted part of the overall extinction spectra. Other components are given to simulate anisotropy of the overall spectrum.

If slightly anisotropic large silver nanoparticles are present while a fraction of the smallest isotropic 10 nm nanoparticles is negligible [Figure 3(*a*)], the spectrum resembles that observed for original experimental samples since the elevated preparation temperature washes out small silver nanoparticles (10–15 nm). The shape of overall extinction spectra *2* in Figure 3(*a*) is broadened, more absorption and scattering occur at the blue end of the spectrum. Further drastic changes in the shape of spectrum *3* in Figure 3(*a*) occur with broadening in a range of 350–550 nm, like for the real spectra in Figure 2; actually its median position at 450 nm corresponds to nothing real since this is a sum curve of different contributions from several fractions of the nanoparticle ensemble. Such a shape evolution has the same tendency as that experimentally observed for the aged samples (Figures 1, 2). Note that this analogy is achieved due to an introduction of a rather small anisotropy of the particles allowing them to contribute to the red shoulder of the spectra. The TEM data (Figure 1) confirm that, indeed, all the samples contain both polyhedral spherical and ellipsoidal nanoparticles while particle size distribution after the ageing of original nanoparticle ensemble (Figures 1, 2) is consistent with the assumptions presented in Figure 3.

Surprisingly, SERS enhancement parameters are not so drastically different for various samples (Figure 4) although particles larger than 80–100 nm do not actually contribute to SERS[20] and this means that aged samples or samples prepared at 40–60 °C could not demonstrate bright SERS spectra. We assume that the contribution of remaining small nanoparticles compensates the lost SERS activity due to the growth of other nanoparticles. Therefore, it is meaningless to correlate artificially the SERS enhancement and the average size of the entire particle size distribution (or plasmonic band position[21]) because the concentration of small nanoparticles seems much more important for SERS.

Thus, the optical properties of the test ensembles of silver nanoparticles allowed us to believe that a mean particle size and

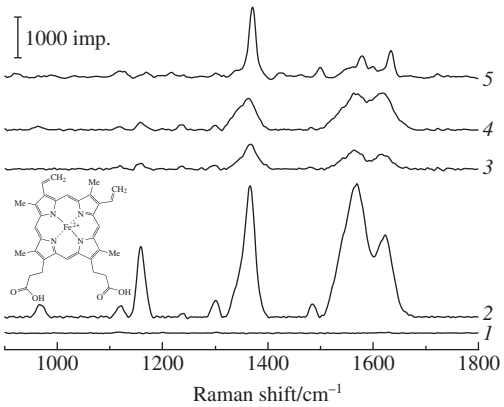

Figure 4 SERS spectra of cytosolic hemoglobin recorded using different hydrosol samples under 514 nm laser illumination. Raman spectra of (*1*) diluted hemoglobin used for SERS measurements and (*5*) the original solution of hemoglobin before dilution, (*2*)–(*4*) hydrosol samples prepared at (*2*) 25, (*3*) 40 and (*4*) 60 °C. The cytosolic hemoglobin was isolated from the cytoplasm of red blood cells taken from male Wistar rats using a phosphate buffer with pH 7.2 and diluted by a factor of 10^4. SERS measurements were optimized for each type of silver nanoparticle sols by adjusting a volume ratio between cytosolic hemoglobin and silver nanoparticle solutions and selection of the highest enhancement factor of the SERS signal. An optimal ratio between silver sols and diluted hemoglobin was 2 : 3. The inset shows the structural formula of heme *b* that gives SERS spectrum of hemoglobin.

the complex morphology is not the only reason for usually observed broad plasmonic peaks but it is particle size distribution peculiarities that contribute substantially to the overall optical properties of the nanoparticles and SERS enhancement parameters.

This work was supported by the Russian Science Foundation (grant no. 14-13-00871) and, in part, by the M. V. Lomonosov Moscow State University Programme of Development for Providing Analytical Research of the Materials.

References

1 J. Kneipp, H. Kneipp, B. Wittig and K. Kneipp, *Nano Lett*., 2007, **7**, 2819.
2 R. A. Álvarez-Puebla and L. M. Liz-Marzán, *Energy Environ. Sci*., 2010, **3**, 1011.
3 L. Polavarapu, J. Perez-Juste, Q.-H. Xu and L. M. Liz-Marzán, *J. Mater. Chem. C*, 2014, **2**, 7460.
4 D. Cialla, A. März, R. Böhme, F. Theil, K. Weber, M. Schmitt and J. Popp, *Anal. Bioanal. Chem*., 2012, **403**, 27.
5 M. Moskovits, *Rev. Mod. Phys.*, 1985, **57**, 783.
6 E. Prodan, C. Radloff, N. J. Halas and P. Nordlander, *Science*, 2003, **302**, 419.
7 A. März, B. Mönch, P. Rösch, M. Kiehntopf, T. Henkel and J. Popp, *Anal. Bioanal. Chem.*, 2011, **400**, 2755.
8 N. G. Khlebtsov, *J. Nanophoton*., 2010, **4**, 041587.
9 Yu. D. Tretyakov and E. A. Goodilin, *Russ. Chem. Rev.*, 2009, **78**, 801 (*Usp. Khim.*, 2009, **78**, 867).
10 E. Yu. Parshina, A. S. Sarycheva, A. I. Yusipovich, N. A. Brazhe, E. A. Goodilin and G. V. Maksimov, *Laser Phys. Lett*., 2013, **10**, 075607.
11 A. A. Semenova, E. A. Goodilin, A. N. Brazhe, V. K. Ivanov, A. E. Baranchikov, V. A. Lebedev, A. E. Goldt, O. V. Sosnovtseva, S. V. Savilov, A. V. Egorov, A. R. Brazhe, E. Y. Parshina, O. G. Luneva, G. V. Maksimov and Yu. D. Tretyakov, *J. Mater. Chem.*, 2012, **22**, 24530.
12 A. A. Semenova, N. A. Brazhe, E. Y. Parshina, V. K. Ivanov, G. V. Maksimov and E. A. Goodilin, *Plasmonics*, 2013, **9**, 227.
13 A. A. Semenova, V. K. Ivanov, S. V. Savilov and E. A. Goodilin, *CrystEngComm*, 2013, **15**, 7863.
14 N. Leopold and B. Lendl, *J. Phys. Chem. B*, 2003, **107**, 5723.
15 B. T. Draine and P. J. Flatau, *J. Opt. Soc. Am. A*, 1994, **11**, 1491.
16 K.-S. Lee and M. A. El-Sayed, *J. Phys. Chem. B*, 2005, **109**, 20331.
17 T. Dadosh, *Mater. Lett*., 2009, **63**, 2236.
18 C. M. Cobley, S. E. Skrabalak, D. J. Campbell and Y. Xia, *Plasmonics*, 2009, **4**, 171.
19 D. D. Evanoff, Jr. and G. Chumanov, *ChemPhysChem*, 2005, **6**, 1221.
20 K. G. Stamplecoskie, J. C. Scaiano, V. S. Tiwari and H. Anis, *J. Phys. Chem. C*, 2011, **115**, 1403.
21 A. V. Sidorov, O. E. Eremina, I. A. Veselova and E. A. Goodilin, *Mendeleev Commun.*, 2015, **25**, 460.

Received: 24th August 2015; Com. 15/4714